https://ntrs.nasa.gov/search.jsp?R=20070017931 2019-08-30T00:45:23+00:00Z

Three-dimensional Computational Fluid Dynamics investigation of a spinning helicopter slung load

J. N. Theron

Northern Arizona University

Flagstaff, AZ, USA, email:jan.theron@nau.edu

E.P.N. Duque

Northern Arizona University

Flagstaff, AZ, USA, email:earl.duque@nau.edu

L. Cicolani

Army/NASA Rotorcraft Division, Ames Research Center

Moffett Field, CA, USA, email: lcicolani@mail.arc.nasa.gov

R. Halsey

Northern Arizona University

Flagstaff, AZ , USA, email: rch23@dana.ucc.nau.edu

Abstract

After performing steady-state Computational Fluid Dynamics (CFD) calculations using OVERFLOW to validate the CFD method against static wind-tunnel data of a box-shaped cargo container, the same setup was used to investigate unsteady

flow with a moving body. Results were compared to flight test data previously collected in which the container is spinning.

Nomenclature

C_DA, C_YA	Drag- and sideforce coefficients	ft^2
C_nA	Yaw moment coefficient (wind axis)	ft^3
$F_{XX}A$, $F_{YY}A$	Body force coefficients	ft^2
M_ZA	Yaw moment coefficient (body axis)	ft^3
Ω	Angular velocity	º/s
A, A_{REF}	Reference area	ft^2
L_{REF}	Reference length	ft
U_∞	Freestream velocity	$ft.s^{-1}$

1. Introduction

Some helicopter slung loads are prone to dynamic instability at airspeeds well below the power-limited speed of the helicopter-slung load configuration [Reference 1]. This includes cargo containers and bluff bodies driven unstable by unsteady aerodynamics. In the absence of realistic models of these aerodynamics, flight tests have been used to validate the safe speed envelopes of helicopter-slung load configurations. This work continues the work done in 2D [References 2 and 3] with the ultimate goal of developing a computational method to predict slung-load instability. We report here on the validation of the 3D CFD method by comparing results against static wind-tunnel data [Reference

4] and expand the steady-state, static CFD analysis to that of a moving body for initial comparison to flight test data [Reference 5]. We present computational fluid dynamics calculations for the 6.41ft x 6.11ft x 8.48ft standard military CONEX cargo container used as a helicopter slung load (Figure 1).

Figure 1 CONEX cargo container

2. Computational setup

2.1 Solver

Prediction of bluff body flow over moving bodies with the associated massive separation requires time-accurate solution of the Navier-Stokes equations. A solution method must be able to accurately capture the viscous boundary layer flow as well as the unsteady and complex shed vortical flow structures. In addition, the method requires the ability to capture unsteady dynamic body motions, either specified or a result from aerodynamic forces.

Very few codes exist, either commercially or within the US government laboratories that can predict such a difficult fluid dynamic problem. Buning, et.al, first developed the OVERFLOW code with fixed wing applications in mind [Reference 6 and 7]. Since then, various versions of the code have been developed and applied to rotorcraft and other moving-body problems [References 8 and 9]. The code's ability to perform arbitrary body motions as demonstrated through various applications including unsteady blade motion of rotorcraft and aircraft store-separation simulations make it the code of choice. For the present work, OVERFLOW version 2.0y was applied. Like other versions of OVERFLOW, this version solves the compressible form of the RANS equations using an implicit finite difference approach with overset grids. The code has various numerical techniques suitable for unsteady flows. The method chosen for this study is a scalar pentadiagonal scheme that is first order accurate in time with 2^{nd} order central differences for spatial terms. To maintain stability, the code uses 2^{nd} and 4^{th} order central difference dissipation terms. Reference 10 presents details on the implicit solution method used by OVERFLOW.

OVERFLOW has several options for modeling boundary layer turbulence. For the studies in this project the Baldwin-Barth (BB) [Reference 11], Spalart-Allmaras (SA) [Reference 12] and the Detached Edddy Simulation (DES) method based upon the SA formulation was used for all the calculations [Reference 13]. The boundary layer was assumed to be fully turbulent. The flow in the background grid was assumed inviscid requiring no turbulence model with the exception of DES-SA. A key feature of this version of the OVERFLOW code is the arbitrary

body motion capability. The current study made use of specified spinning motions of a rectangular box representative of the CONEX.

2.1 Clusters and benchmarking

Calculations were performed on small clusters of dual-CPU nodes and the Columbia high-performance computer located at NASA Ames. Unsteady calculations are very compute-intensive and the performance of these clusters using Overflow 2 are included in Table 1:

Table 1 High performance computers used in this study

	Columbia	**NAU xbot**	**NAU phoebe**
CPU	Itanium2	Apple PPC 970	AMD Opteron
Compiler	Intel	XLF / gcc	PGI
CPUs used	28	4	16
Performance[A]	0.3	2.2	1.4
Time per CONEX revolution[B]	1.8	13.2	8.4

A: Units of measure: $\mu s.step^{-1}.gridpoint^{-1}$, B: wall hours

2.2 Computational grids

Given the assumption that the forces and moments experienced by a bluff body that is subject to massive separation should be fairly insensitive to small details, the actual body can be approximated by a simplified geometric shape. For the present computation, the CONEX is represented by a box 8.48ft wide by 6.11ft deep by 6.41ft high. Omitted details are skids, sidepanel corrugations, and an

indentation around the top edges - a future study will use grids that model these details. A periodic surface grid with two axis points and dimensions J=181, K=301, L=1 (J from axis to axis, K around the perimeter and L outwards normal to the surface) was projected onto this shape. This surface grid was then marched out hyperbolically in the +Z direction to create a near-body (NB) grid that consists of 29 layers with the first ten equispaced at 3E-5 ft (y^+=1) and the last nineteen stretched to a spacing of 0.15ft at a distance of 1.5ft from the surface. Figure 2 shows a close-up of the CONEX grid system.

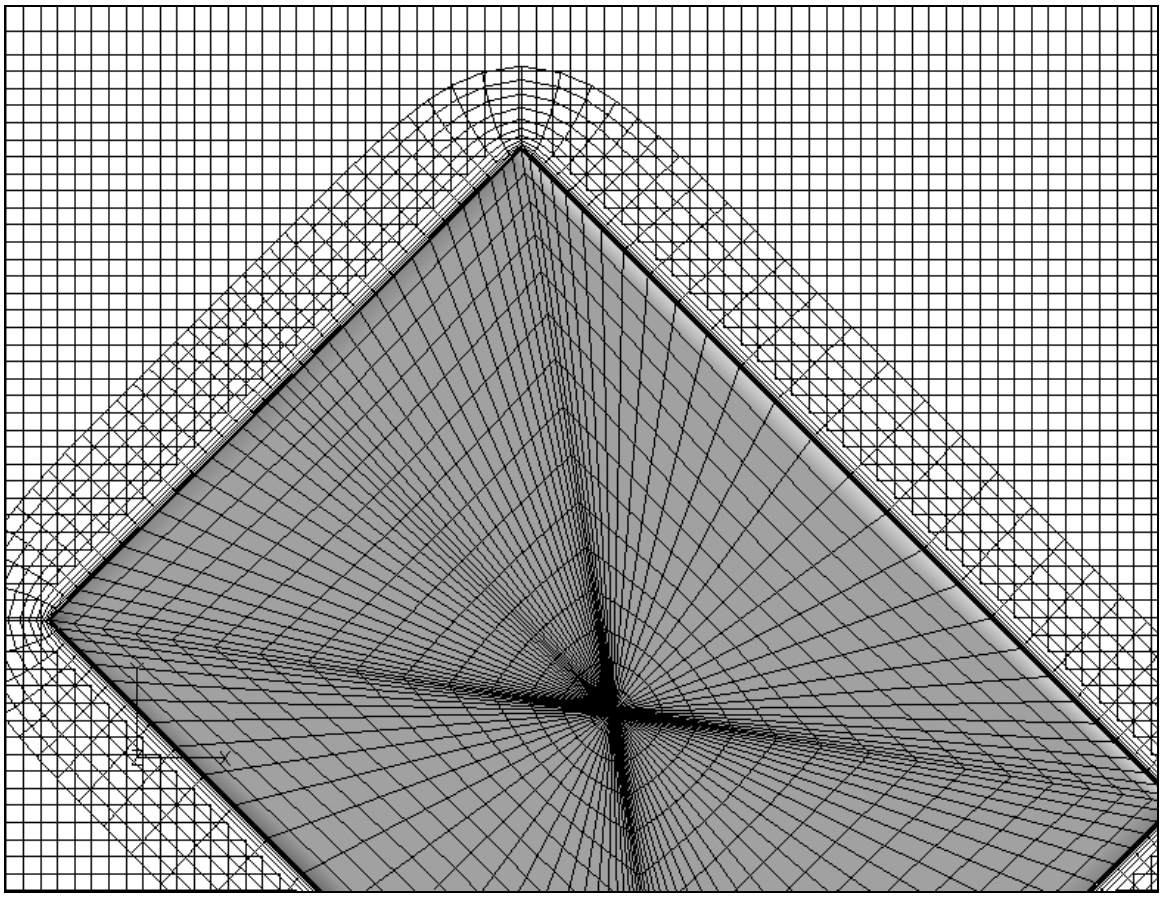

Figure 2 Details of the CONEX grids (every 2nd point shown) viewed from +Z. Flow is left to right, X axis to the right, Y axis to the top of the image.

The remainder of the computational domain was filled with a single structured grid consisting of an unstretched region (± 6ft in five directions and +12ft in the +X direction from the origin) around the NB grid and a stretched region to a distance of 80ft from the origin in all six directions. The stretching ratios of the stretched portion of the grid were 1.2 in the X direction and 1.3 in the Y and Z directions (see **Error! Reference source not found.** for a close view of the off-body grid in the region of the CONEX near-body grid). Overflow uses xrays to cut a hole in the off-body grid for the overset-grid method. We used a total of 5E6 grid points for the steady-state study and refined the off-body grid slightly for the unsteady runs, resulting in about 6E6 grid points. A dimensionless timestep equivalent to 7E-4s and double-precision grids were found to give reproducible results in unsteady simulations. We found no significant difference in results when using single-precision grids for steady-state runs.

3. Results

In this section we consider validation of the CFD method against static aerodynamic wind tunnel data [Reference 4] and a limited amount of recent (unpublished) flight data. The wind tunnel data is given every 5° over the complete angle of attack and sideslip domain. The balance and sting were developed to eliminate errors revealed by departures of the data from the zeros that should occur in the forces and moments at certain orientations of a smooth cubic test model. In flight, the CONEX suspended with a swivel adopts a steady

spin rate that is a function of airspeed. Spin rates over 150º/s were observed. The load was instrumented sufficiently to determine X and Y body forces and Z body axis yaw moment. While measurement errors in the flight data have not yet been evaluated, the data shows a reasonable relationship to the static wind tunnel data.

3.1 Validation against static wind tunnel data

The first step in our validation was against wind tunnel data previously collected at the Technion-Israel Institute of Technology [Reference 4]. The WT data was taken using a detailed CONEX model with skids, corner indentations as well as side-panel corrugations (see section 3.3), while the CFD data was computed for a box without details. All steady-state CFD results are at 0° angle of attack.

The wind-tunnel (WT) force and moment components were found to be periodic every 180º in sideslip angle and related every quadrant by symmetry rules. Hence, the CFD analysis was set up to calculate forces and moments in the first quadrant every 5º from 0º to 90º. The CONEX was maintained at a constant sideslip angle (β) and with the solver set to steady-state mode, 4,000 timesteps were calculated. Even after 4,000 timesteps, the forces and moments did not converge to a unique value. This is not surprising, considering the nature of the flow; i.e. massive separation and vortex shedding as shown in **Figure 3**.

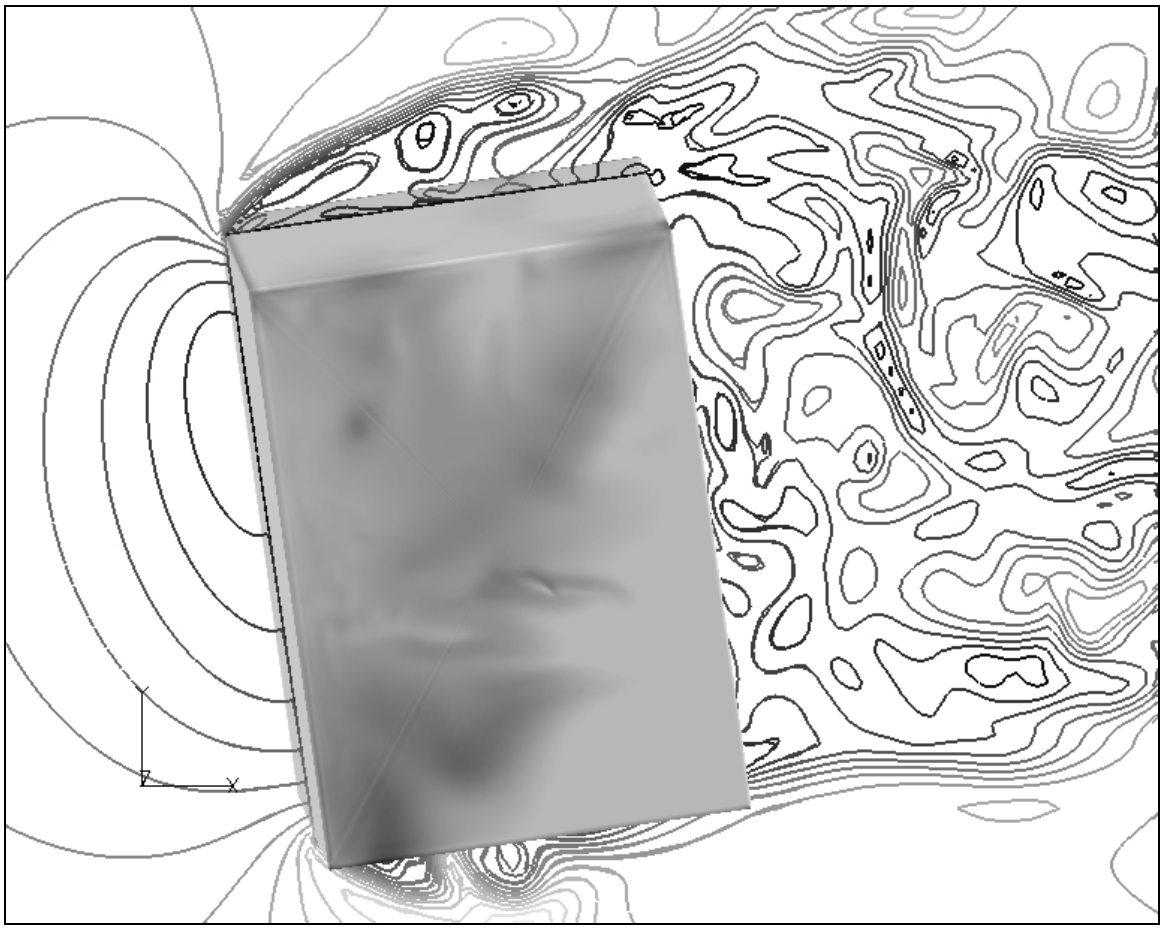

Figure 3 Flow field (velocity contours) of rotating CONEX. The surface is shaded with pressure

Smaller timesteps did not alleviate this apparent lack of convergence. Consequently, the steady state results are in fact time-averaged values over 4,000 “steady-state” timesteps.

Four turbulence models were evaluated, namely BB, SA, kω and kω-SST. The latter two models are two-equation models that were developed to better resolve shear layers and separated flow. Results compared to wind tunnel data are

shown below. For drag (Figure 4), all turbulence models predict similar C_DA at sideslip angles between 30° and 75°, but major differences arise at low and high sideslip (broad side and narrow side to the wind respectively). BB appears to be the only model that follows the wind-tunnel variation (albeit somewhat offset from the measured data) correctly at both extremes. The two-equation models fare the worst with kω exhibiting the highest discrepancy with WT data at most sideslip angles studied. It does appear that kω-SST improves on the performance of kω. We do not rule out the possibility that these results may be improved upon by further refinement of the grids, timestep and numerical techniques employed; however, since the objective of this work is the unsteady prediction of aerodynamic properties of the CONEX, steady-state results were accepted as-is for validation purposes.

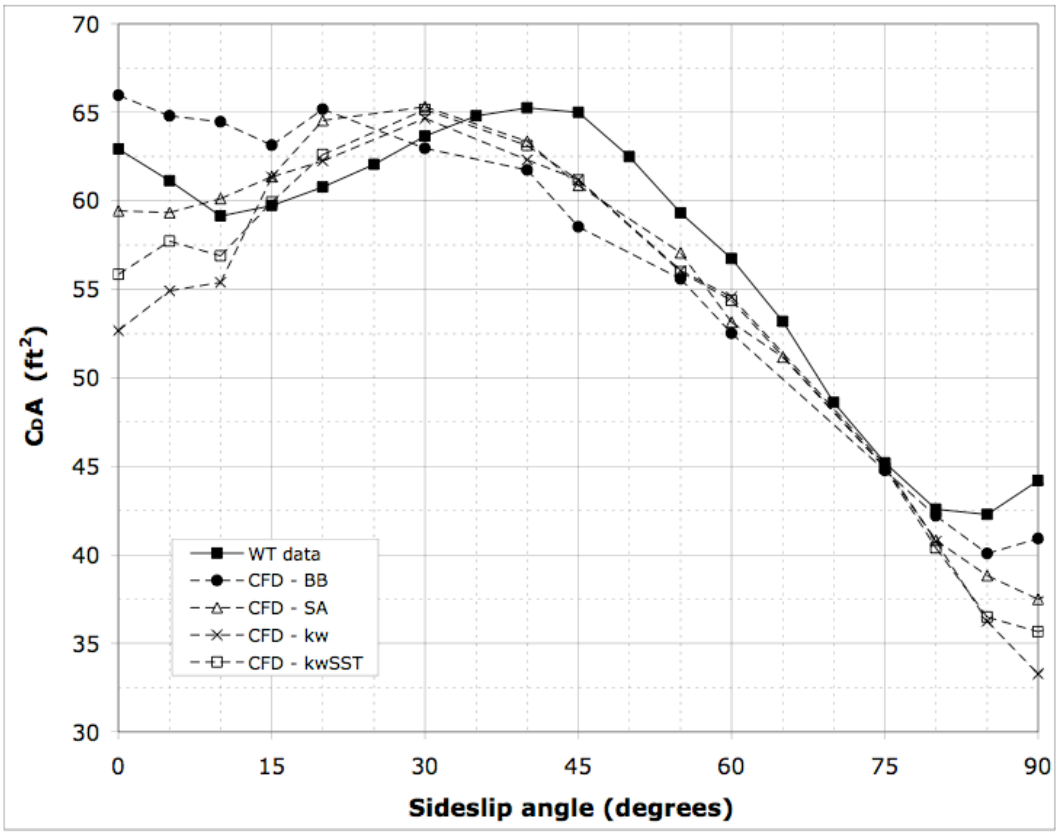

Figure 4 Steady-state drag force (C_DA) compared to wind tunnel data

For side force (Figure 5) the worst predictor is the kω model which deviates from WT data both at low and high sideslip angles. The kω-SST model does improve on this performance, but results are as good as and no better than that predicted by the one-equation models (BB and SA). Between 60° and 90°, all models fail to accurately follow the sharp decline in side force measured in the wind tunnel.

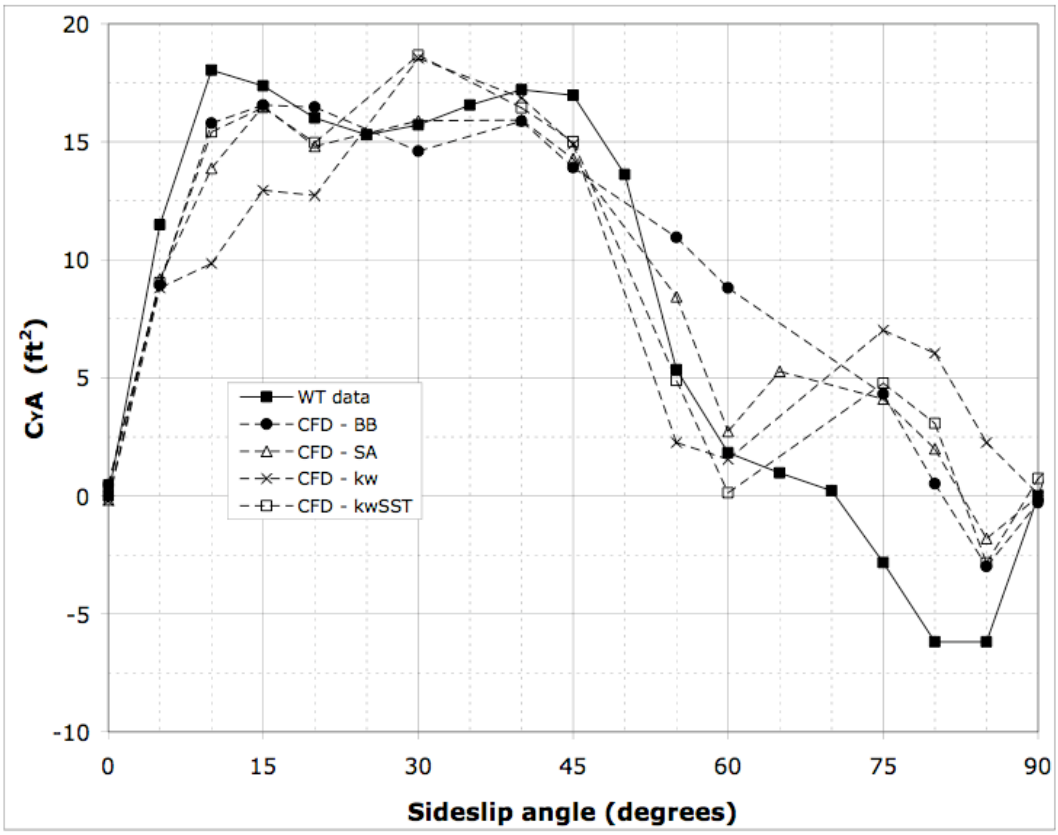

Figure 5 Steady-state side force ($C_Y A$) compared to wind tunnel data

The BB turbulence model is able to predict the yaw moment measured in the wind tunnel most accurately of the turbulence models used in this study. The kω and kω-SST turbulence models show the highest deviation from measured data.

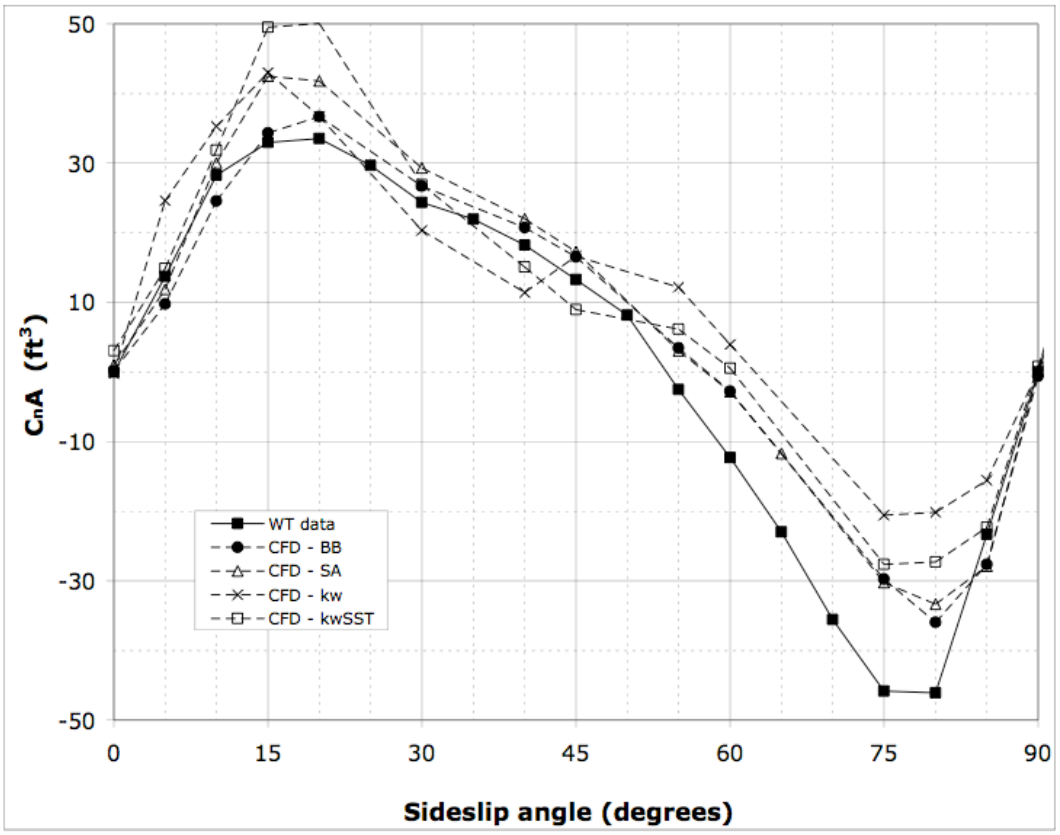

Figure 6 Steady-state yaw moment (C_nA) compared to wind tunnel data

In summarizing these results, the root mean square errors (RMSE) were calculated for each of the turbulence models for the three aerodynamic coefficients (drag force, side force and yaw moment) and compared to find the most appropriate turbulence model to use for the remainder of the study. This is summarized below in Table 2.

Table 2 Comparison between steady-state CFD data and wind tunnel results

	RMSE			
Turbulence model	**C_DA**	**C_YA**	**C_NA**	**Total**
	% of avg.	% of max.	% of max.	
Baldwin-Barth	6.45	21.55	***19.07***	***31.09***
Spalart-Allmaras	***5.75***	25.04	40.95	55.37
kω	9.02	31.24	37.45	54.83
kω-SST	7.04	***20.23***	31.23	44.02

For the CONEX used in slung-load configuration the major unstable motion is yaw around the CONEX center of gravity (C.G.). BB is the best predictor of yaw moment by far. SA does best at drag force while the side force is best predicted by the kω-SST model. Since one is very unlikely to use more than one turbulence model for a single problem in practice, we summed all the squared errors (for C_DA, C_YA and C_NA) and took the square root to obtain a measure of the overall performance of each model (last column in **Table 2**). The fact that the BB turbulence model performs the best overall by a significant margin is a surprising result, taking into account the claim that two-equation turbulence models are better able to resolve separated flow. However, considering the massive separation taking place here there must be doubt whether the parameters of these models have been appropriately tuned for such a flow type.

3.2 Moving CONEX

The Baldwin-Barth turbulence model was used for the unsteady part of this study, based on validation against wind tunnel results shown earlier. Initial unsteady runs showed that a timestep corresponding to 0.1° of rotation is sufficiently small to result in a periodic solution after less than one revolution (see Figure 5). Larger timesteps and single-precision grids resulted in significant variation of calculated forces and moments from one revolution to the next.

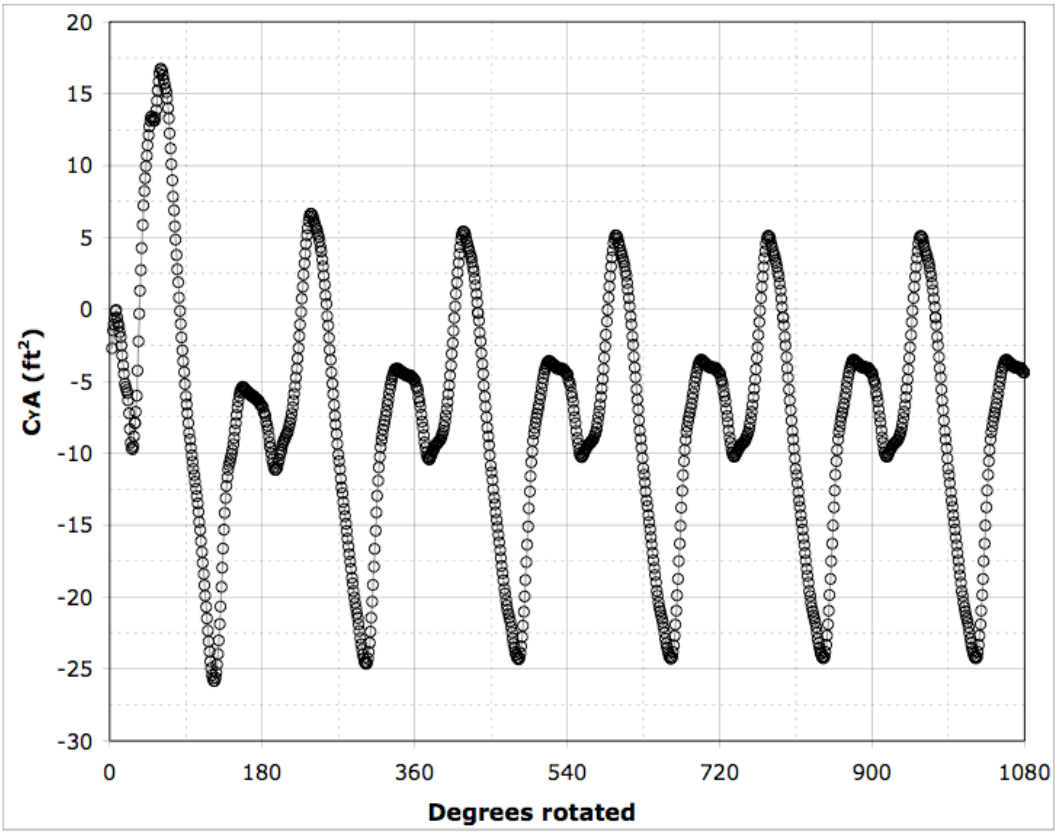

Figure 7 Side force (α=0°, Ω*=150°/s) calculated over three CONEX revolutions

3.2.1 Constant yaw rate at zero pitch angle

In order to establish the effect of the rotating CONEX on its aerodynamic properties compared to its static aerodynamics as measured in the wind tunnel and validated with steady-state CFD, three constant-rate rotations around the Z axis (yaw) were studied, namely 50, 100 and 150°/s at 60 ktas. The results are presented for drag coefficient (C_DA), side force coefficient (C_YA) and yaw moment coefficient (C_nA) and are compared to wind tunnel data.

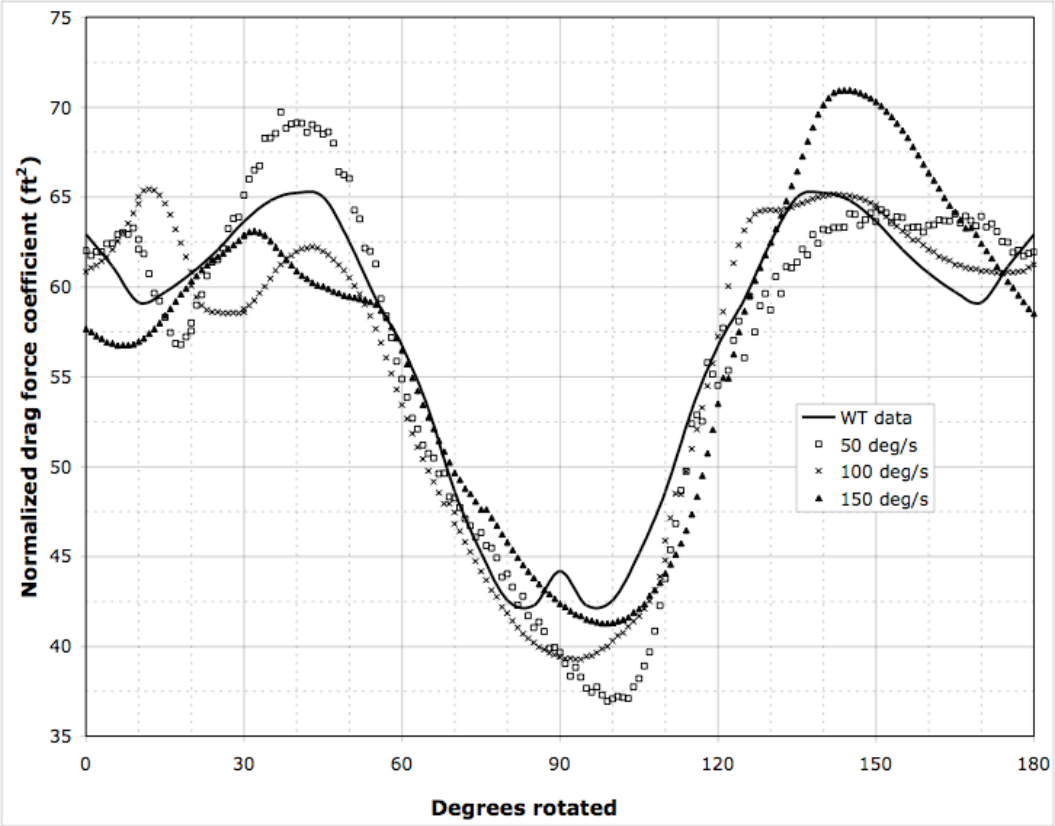

Figure 8 Comparison of drag force (C_DA) between stationary WT data and moving-body CFD results (aoa=0°)

As the CONEX starts to rotate at higher angular velocities, the drag force (C_DA) loses the symmetry around 90° observed in the WT and steady-state CFD data.

The peak at 45° that is evident at Ω=50°/s disappears in favour of an enhanced peak at 135° at Ω=150°/s. No discernable trend with respect to the phase lag is evident.

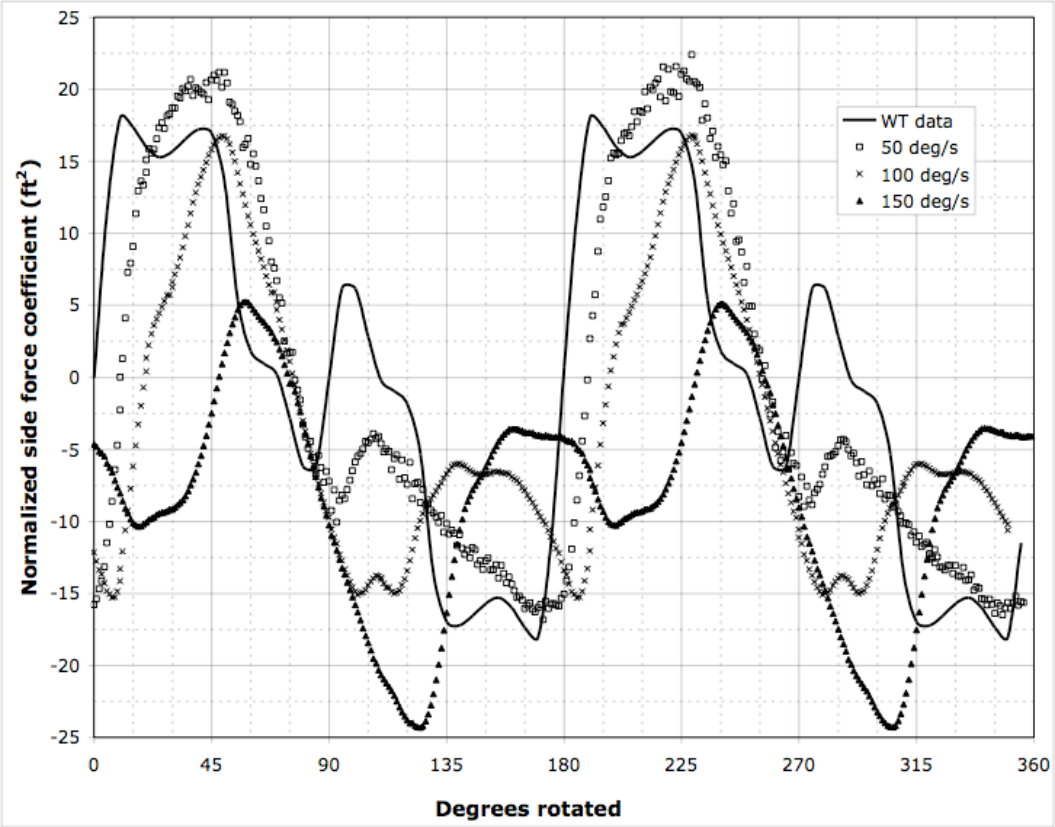

Figure 9 Comparison of side force (C_YA) between stationary WT data and moving-body CFD results (aoa=0°)

In contrast to C_DA, the side force (C_YA) exhibits large deviations from the static aerodynamics when the CONEX starts to rotate. At Ω=50°/s, the CFD data resembles the static aerodynamics, but as Ω increases, CFD results starts to deviate substantially in a number of ways. Firstly, the major peaks start to shift to

the right, indicating a phase lag which appears to be consistent with angular velocity. The minor peak at about 100º diminishes and eventually disappears.

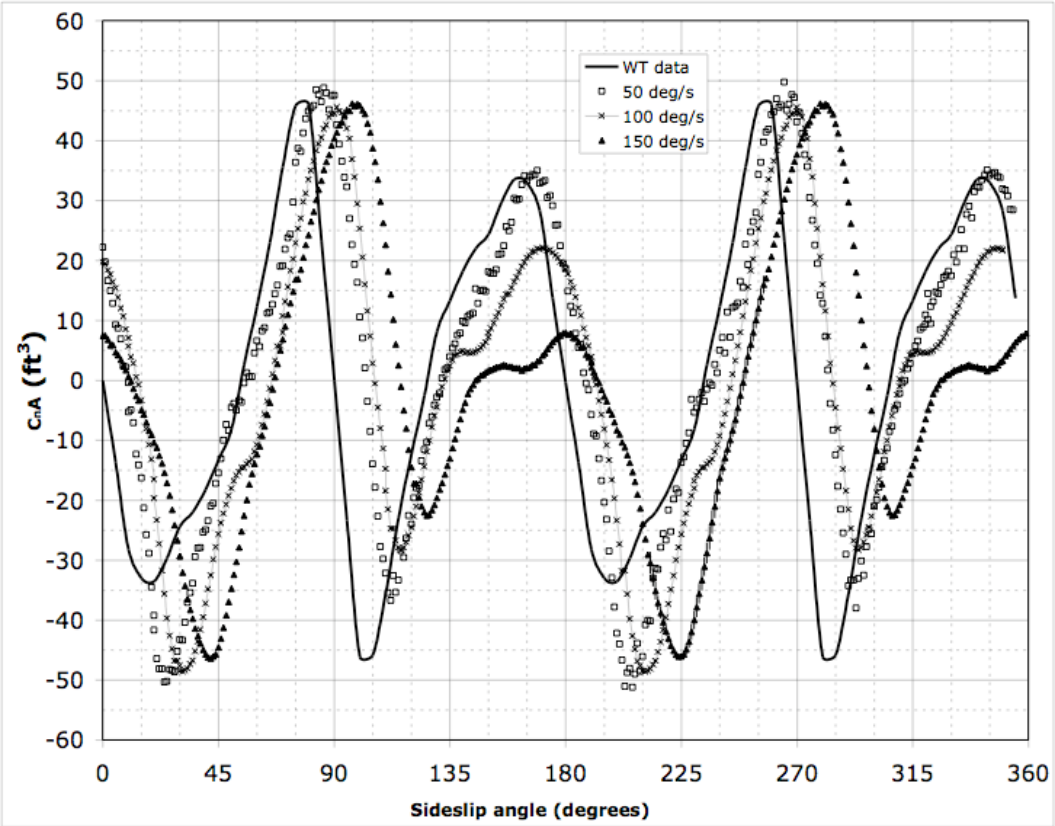

Figure 10 Comparison of yaw moment (C_nA) between stationary WT data and moving-body CFD results (aoa=0°)

The CFD-predicted yaw moment (C_nA) exhibits a phase lag with respect to steady-state data, increasing with angular velocity to about 25º at an angular velocity of 150º/s. An interesting phenomenon is the fact that the magnitude of the major peaks at 90º and 270º do not change with Ω, while all other peaks (positive and negative) exhibit a shift in magnitude which is a function of the angular velocity.

Based on these promising results, the CFD method and box-like grid was compared to flight test data collected on the full-scale CONEX.

3.3 Comparison with flight test data

Flight tests conducted at NASA Ames indicated that the CONEX suspended with four sling legs attached to a single hook point from a Black Hawk UH60A exhibits three simple modes of body motion [Reference 1], most of which are strong functions of CONEX weight and true airspeed. First, the CONEX trails behind the hook point at an angle; at 60 ktas the angle is about 11° from the vertical. Secondly, it rotates about the hook-CONEX-cg line segment at a steady angular velocity; at 60 knots, this rotation rate is about 157.6°/s. The third mode is a limit-cycle pendulum motion of about ± 3° about the 11° trailing angle. The overall effect of these three motions is that the CONEX CG follows the path ascribed by the rim of an inverted cone while the CG rotates about the line that connects the rim of the cone to its base. One of the main goals of this work was to arrive at a computational setup that would be able to predict the aerodynamic forces and moments of the CONEX during this steady, cyclic rotation. The amplitude and period of the pendulum motion, the spin rate and the trailing angle are functions of airspeed and CONEX weight. The objective of this work is to define an aerodynamic model for rigid body simulations of the (12DOF) slung load system.

The flight test data was obtained with an instrumented load but without hook force measurements. Consequently, the aerodynamics that could be derived from the data are limited to body axes X and Y force components (components perpendicular to the hook force vector - $F_{XX}A$ and $F_{YY}A$) and the Z-body axis moment (moment about the direction of the hook force - M_ZA). Tests are in progress that will include hook force measurements.

The present CFD computations approximate the flight condition. The CFD data simulate the CONEX spinning at 150°/s about the Z axis. There are small mismatches from the flight case spin rate (158°/s), the limit cycle is omitted, and some CONEX structural details are omitted in the CFD model.

For the body X force (Figure 11) there is excellent agreement between CFD and flight data, especially considering the simplification of the CONEX in the CFD model. The CFD method was able to capture the major phenomena, although peak values are somewhat over-predicted and minima under-predicted.

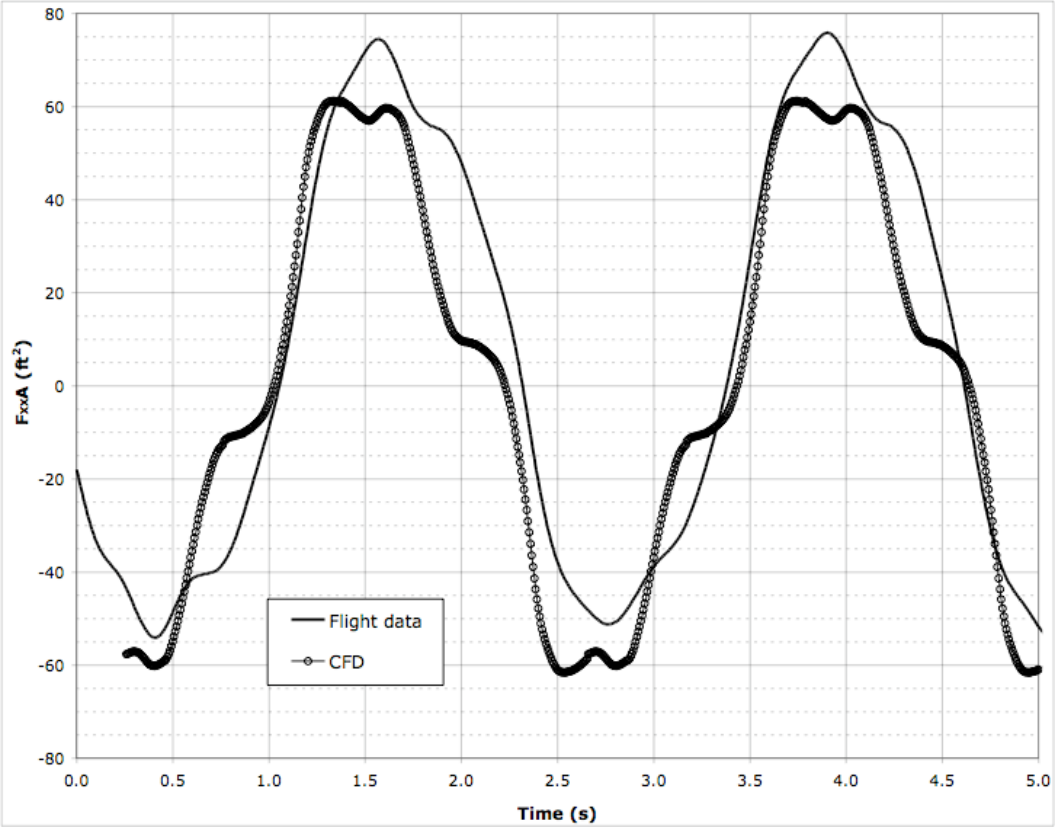

Figure 11 Comparison of $F_{XX}A$ from flight data with unsteady CFD

Further CFD tests at 157.6°/s are expected to shed more light on the presence of and magnitude of the shoulders.

$F_{YY}A$ is also fairly well predicted, although there are extra peaks in the CFD solution that are absent from flight test data. A closer look at flight data leads one to believe that such double peaks may be present in the data, but if so, are certainly of much smaller magnitude than the predictions from CFD simulations would lead one to believe.

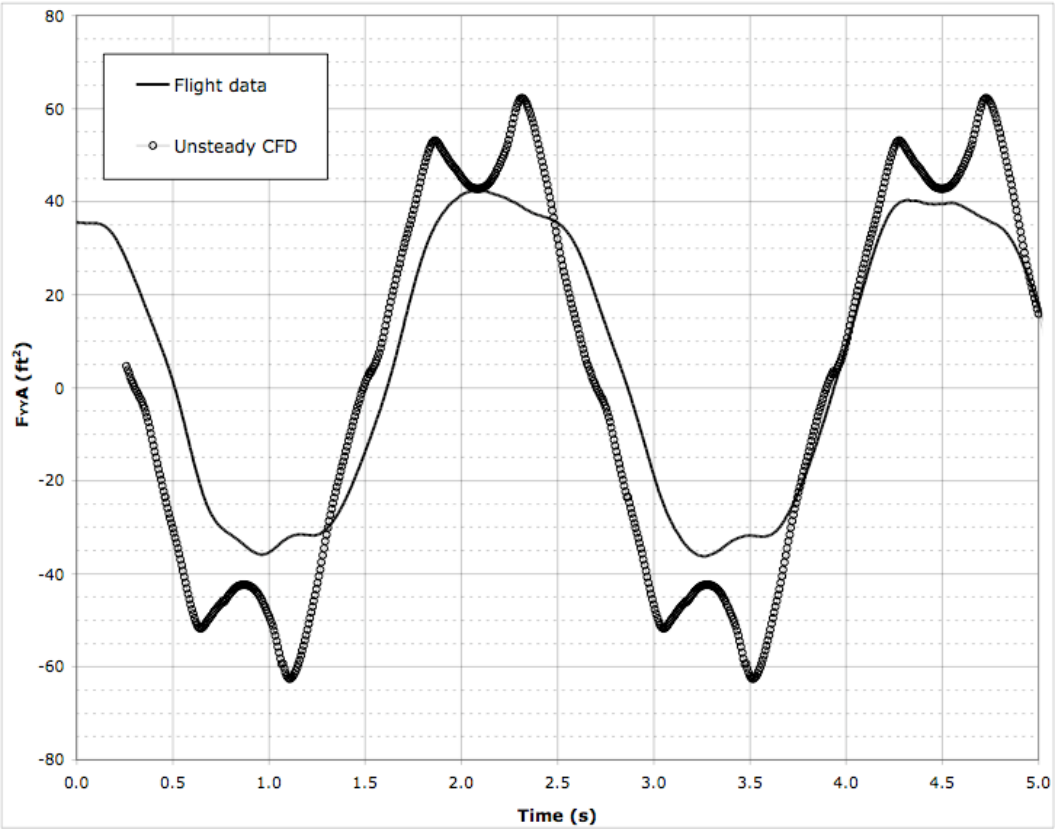

Figure 12 Comparison of $F_{YY}A$ from flight data with unsteady CFD

The difference in rotation rate between the CFD test and flight data is most apparent in the yaw moment (M_ZA) data presented in Figure 13 where the phase shift is obvious. In this case, the maxima and minima are overpredicted and in the CFD data there is a shoulder present on the secondary maximum that is not apparent from flight data.

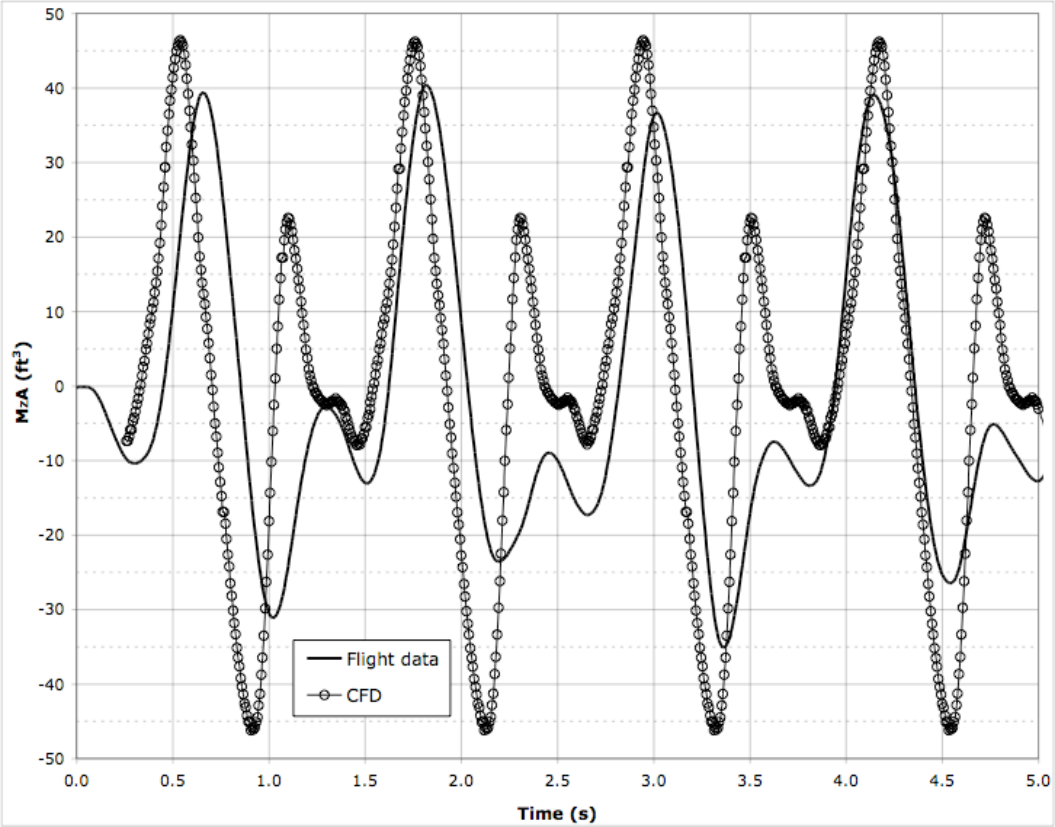

Figure 13 Comparison of $M_Z A$ from flight data with unsteady CFD

The difference in magnitude of the primary minima in Figure 13 may be due to the omission of the limit cycle pendulum motion in the CFD experiment. In the future, this comparison will be recomputed with more exact reproduction of the flight motion.

5. Conclusions

We developed a 3D CFD method and a simplified grid to represent the full-scale CONEX and validated the grid and solver against wind tunnel data in steady-state mode. The authors subsequently used this grid and, with a simplified

version of the actual body motion experienced by the CONEX during full-scale flight tests then prescribed to the grid, calculated the forces and moments in an unsteady CFD simulation. Results compared very well with flight test data, considering the sweeping assumptions made about the geometry and the simplified body motion used to mimic flight conditions. Future work will include prescribed-motion CFD simulations using the full body motion measured during flight, more detailed models of the geometry and a number of frequency sweeps to elucidate major aerodynamic phenomena.

Acknowledgements

This work was funded by NASA contracts NNA04CK19G and NNA05CS80A and conducted under the Army-Israel Memorandum of Agreement for cooperative research on "Rotorcraft Aeromechanics and Man-Machine Integration technology". The authors would like to acknowledge the generous contributions and technical guidance from Dr. Mark Tischler, Dr. Shlomit Gali and Prof. Aviv Rosen.

References

1. Tyson, P., "Simulation validation and flight prediction of UH-60A Black Hawk helicopters/slung load characteristics," M.Sc. Thesis, Naval Postgraduate School, U.S. Naval Academy. March 1999
2. da Silva, J.G.A., Duque, E.P.N., Cicolani, L.S. and Tischler, M.B., "Unsteady aerodynamic model of a cargo container for slung-load simulation," *29th European Rotorcraft Forum*, Sept 2003, July 2004, p. 357
3. Cicolani, L.S., da Silva, J.G.A., Duque, E.P.N., and Tischler, M., "Unsteady Aerodynamic Model of a Cargo Container for Slung-Load Simulation: Preliminary Aerodynamic Data and Model Identification," NASA/TP-2004-

212817, May 2004 also published in *The Aeronautical Journal*, July 2004, p. 357
4. Rosen, A., Cecutta, S., Yaffe, R., “Wind Tunnel Tests of Cube and CONEX models,” Faculty of Aerospace Engineering, Technion-Israel Institute of Technology, Haifa 32000 Israel ,TAE 884 (November, 1999)
5. Cicolani, L.S., McCoy, A.H., Sahai, A.H., Tyson, R., Tischler, M.B., Ronen, A. and Tucker, G., “Flight test identification and simulation of a UH-60A helicopter and slung load”*, J. American Helicopter Society*, 2001, 46, pp. 140-160
6. Buning, P.G., Chiu, I.T., Obayashi, S., Rizk, Y.M. and Steger, J.L., “Numerical simulation of the integrated space shuttle vehicle in ascent”, AIAA 88-4359, AIAA Atmospheric Flight Mechanics Meeting, Minneapolis, MN, August 15-17, 1988
7. Buning, P.G. Jespersen, D.C., Pulliam, T.H., Klopfer, G.H., Chan, W.M., Slotnick, J.P., Krist, S.E. and Renze, K.J., *Overflow User’s Manual* Version 1.8aa, 24 April 2003
8. Ahmad, J. and Duque, E.P.N., "Helicopter Rotor Blade Computation in Unsteady Flows Using Moving Overset Grids," Journal of Aircraft, Vol. 33, No. 1, pp. 54-60, January-February 1996
9. Meakin, R., “Moving grid overset grid methods for complete aircraft tiltrotor simulations”, AIAA 93-3350, July 1993
10. Pulliam, T.H. and Steger, J.L., “Implicit Finite-Different Simulations of Three-Dimensional Compressible Flow,” AIAA J. Vol. 18, No. 2, p. 159, February 1980.
11. Baldwin, B.S. and Barth, T.J., “A One-Equation Turbulence Transport Model for High Reynolds Number Wall-Bounded Flows,” NASA TM 102847, August 1990.
12. Spalart P.R., Allmaras S.R., “A One-equation Turbulence Model for Aerodynamic Flows,” 29th Aerospace Sciences Meeting, Reno, NV, AIAA-92-0439, January 1992 12 Menter, F R. “Two-equation Eddy-viscosity Turbulence Models for Engineering Applications,” AIAA Journal vol. 32 no. 8, 1994 pg 598-605
13. Strelets M., “Detached Eddy Simulation of Massively Separated Flows,” 2001, AIAA Paper 2001-0879